RESERVOIR CHARACTERIZATION OF THE HORN MOUNTAIN OIL FIELD, MISSISSIPPI CANYON, GULF OF MEXICO

A Thesis

by

YUJIA LI

Submitted to the Office of Graduate and Professional Studies of
Texas A&M University
in partial fulfillment of the requirements for the degree of

MASTER OF SCIENCE

Chair of Committee,	Michael Pope
Committee Members,	Walter Ayers
	Richard Gibson
John R. Giardino,	Head of Department

May 2015

Major Subject: Geophysics

ABSTRACT

Horn Mountain Field is a mid-sized oil and associated gas field located in the northeastern corner of Mississippi Canyon, Gulf of Mexico. Production at Horn Mountain Field declined significantly since 2006 with an increased water cut in most wells. Boost in production is expect with some new wells and mid-life work. To assist the rework of the field and plan for future development, characterization of the reservoir is necessary. This study is based on geologic interpretation of a seismic volume and well log data. A model was built based on the interpreted faults and horizons using PETREL^{TM} software.

Horn Mountain field mainly produced from two Middle Miocene sands: J and M sands. J sands were interpreted to be deposited in a relatively confined levee channel with lower Net-to-Gross ratio (N/G; ~15-40%) and M sands formed a confined channel with N/G (20-80%). The field is divided in to three main fault blocks: north fault block (NFB), central fault block (CFB) and eastern fault block (EFB). J sands juxtapose across the fault that separates CFB and EFB where different OWC were identified, which indicates hydrocarbon generated from source rock migrating along major bounding fault to the north, where NFB was charged then subsequently spill to CFB and EFB. It also indicates stratigraphic barrier in J sands.

The total deterministic volume is calculated based on a model. The model was built from the well-top depth controlled seismic interpretation, where N/G was calculated based on correlation between seismic amplitude and well log N/G observation and reservoir parameters from well logs. Model based calculation indicates that the

recoverable oil is 26 MOBE for J sands and 127 MOBE for M2 sands, which is the main contributor from stacked M sands. Over half of the reserves for both J and M sands are within NFB, and around 30% in CFB. Only one well produced the down-dip portion of M2 from the EFB. There is potentially 4 MOBE from J sand and 22 MOBE recoverable from M2 in EFB, where the 4 MOBE of J sands was not penetrated (tested or produced) based on the data available. Future development of the unpenetrated block should significantly increase the future production with near field development.

ACKNOWLEDGEMENTS

I would like to thank my committee chair, Dr. Pope, and my committee members, Dr. Ayers, Dr. Gibson, for their guidance and support throughout the course of this research.

Thanks also go to my friends and colleagues and the department faculty and staff for making my time at Texas A&M University a great experience. I also want to extend my gratitude to the BP Inc., which provided the seismic and well log data. I would like to thank my colleague, Dionisio Custodio at ExxonMobil Corp., for his technical guidance with PETREL modeling. Finally, thanks to my husband and my parents for their encouragement and support through the years.

DEDICATION

The thesis is dedicated to my teacher and friend, Dr. Wayne Ahr, who had devoted his life to advancing our understanding of carbonate rocks and to mentoring new generation of geoscientists.

TABLE OF CONTENTS

LIST OF FIGURES

LIST OF TABLES

1. INTRODUCTION

The cost of exploration, development and production of petroleum fields in deep water is very high compared to onshore or shallow water regions. Typical development cost for deep water discoveries average over $850 million (Bramlett and Kendrick, 2000) and this number continues to increase. Capital investment for deep water development grew from $40 billion in 2005 up to $70 billion in 2010 (Little, 2013), From 1975 to 2010, there were at least 285 deep water discoveries in the Gulf of Mexico (GoM), of which 127 became proven fields, accounting for 11.060 BBOE of proved reserves (OCS Report, 2009). Development wells cost one-third to one-half of a field's development cost (Kendrick, 2000). Therefore, it is critical to carefully study potential fields for their structural framework and reservoir properties distribution by combining 3-D seismic and well log data. An accurate reservoir model with available data will greatly help in designing wells that can deliver enough oil and gas at sufficient and sustained rates to achieve commercial success.

Horn Mountain (GoM block MC 126 and MC 127) is a medium-sized oil and associated gas field located in the northeastern corner of the Mississippi Canyon protraction area (Fig 1). The northwestern field extension lies partially in GoM block MC 82. It is 100% owned and operated by Plains E&P, who acquired the asset with facilities from BP in 2012 as part of a wider deal in deepwater Gulf of Mexico. Horn Mountain was developed using a truss-type spar with eight producers and two water injectors; first production occurred in November 2002.

The Horn Mountain field produces from two Middle Miocene reservoirs. The Horn Mountain field is compartmentalized into three major producing blocks divided by major faults (Milkov et al., 2007). Flow baffles occur between wells producing in the same field. To refine the compartmentalization model, seismic attribute analysis was performed to study the fluid distribution. Seismic features such as bright/dim/flat spots may provide important insights into compartments connectivity, charging history and characteristics and hydrocarbon potential beyond the current producing compartments (i.e., un-drained compartments). Seismic attributes also are very useful to understand the 3-D architecture of the field.

The study presents the results of reservoir characterization based on 3-D seismic interpretation and well log integration from Horn Mountain field, deepwater GoM and using an industry work flow. Four key horizons were mapped for the main producing intervals: J-Sand top and base, and M2-Sand Top and Base. We characterize the J and M2 reservoirs and determine the correlation of seismic attributes and reservoir quality and build a PETREL^{TM} model with environment of deposition (EOD). We also estimate volumes of hydrocarbon remaining based on the model with variable reservoir properties and discuss implications for a future field development plan.

2. REGIONAL GEOLOGY

The Gulf of Mexico is characterized by a Jurassic to Pleistocene sedimentary succession formed by initial rifting of North America from South America followed by drifting of its passive margins (McDonnell et al. 2008). Mississippi Canyon is located to the southeast of Louisiana in the north-central GoM. This is an underwater canyon formed as part of the Mississippi Submarine Valley. Horn Mountain field (Fig. 1) is located in Mississippi Canyon blocks MC 126 and MC 127 of north-central GoM at a water depth of around 5422 ft (1653 m). Topographic map shows the location of Horn Mountain field near the Dorsey deep sea canyon, which is an over 400 m deep valley extending 60 km basinward, surrounded by round, flat-topped domes supported by salt bodies below (Sylvester et al. 2012; Continental Shelf Associates, Inc. 2000). Four salt domes are recognized, two to the east of the canyon and two to the west of the canyon (Fig. 2a). Seismic line A-A' shows the northwest salt canopy, where the canyon and a deep salt pillow are recognized (Fig. 2b); seismic line B-B', shows the northwest and southwest salt domes (Fig. 2C).

The major reservoir intervals are Miocene amalgamated channel/slope canyon deposits and associated submarine fan complexes deposited in a passive margin unconfined slope setting (Clemenceau and Miller, 1993; Clemenceau et al, 2000; Pfeiffer, 2000). The reservoirs are sandstone of submarine channel facies interbedded and laminated sandstone of levee facies with shale based on core observation. There are two shallow salt canopies (< 9000-5000 ft below sea floor) to the south and north of Horn Mountain and a salt structure at depth of ~20,000 ft (Fig. 2).

Regional faults strike mostly northeast-southwest. These faults are probably a combination of detachment faults caused by the salt mobilization similar to these of the western GoM (McDonnell et al., 2008), and growth faults at the crest of the deep salt canopy. The field was discovered in July 1999, and started to produce in November 2002. In 2008, the field had a capability of producing 75,000 bopd, 72 mmscfd including gas lift, and 25,000 bwpd. By 2008, the field had produced approximately 102 MBOE gross (BP management review, 2008).

Previous studies showed that the reservoir has porosity ranging from 20-35% with an average porosity at 28% and an average water saturation of 25% (BP management review, 2008). The permeability ranges from 100-6,000 md. Oil produced is 34-37 degree API.

In Horn Mountain oil field, the pay intervals are located between 12,200 and 14,200 ft (3719 and 4328 m) true vertical depth subsea (TVDSS). Two major pay intervals J (shallower) and M (deeper) were identified (Fig. 3), with M sand containing 124 MBOE (82% of the reserve) and J sand 27 MBOE (18% of the reserves).

Horn Mountain field consists of two stacked Middle Miocene reservoirs (Milkov et al., 2007). The reservoirs form a gently south and southwest dipping structure with up-dip faulting and thinning. Hydrocarbon in Horn Mountain field is trapped within channel sands by a combination structural / stratigraphic mechanism, and several smaller faults and depositional features (channel boundaries and overbank facies) appear to separate both sands into northern, central and eastern fault blocks. Reservoir M is subdivided into three zones M1, M2 and M3 vertically from the top, with M2 being most

extensive and productive. Thinner and discontinuous interval K between M and J pay intervals contains only gas as indicated by well log data. It is not laterally extensive and is not currently producing.

Reservoirs M and J are bounded by a regional west-east trending fault that dips steeply to the north and a stratigraphic pinch-out in the eastern and northeastern part of the field. The hydrocarbon was trapped by a series of normal faults, which separated the field into several fault blocks. The major producing field is in the southern portion of the field (Milkov et al., 2007). The producing field is divided by regional faults into a CFB, NFB and EFB (Fig. 4).

Based on the pressure data, seismic amplitude data, pressure-volume-temperature relationships (PVT data), including gas-oil ratio (GOR) and API data, and geochemistry data (oil fingerprints and gas isotope data), the field is compartmentalized into sections divided by low, moderate and high risk flow barriers. The major flow barriers are structural, which includes the major faults, and moderate flow barriers are stratigraphic, including the overbank and levee facies between slope channels (Milkov et al., 2007).

A petroleum migration model was proposed based on the hydrocarbon maturity indicators (Milkov et al., 2007). It was proposed that microbial gas fills part of both M- and J-reservoirs before the entry of thermogenic petroleum from the underlying Eocene to Jurassic source rock (Hood et al., 2002). First, undersaturated oil filled the CFB of the M-reservoir, dissolving the microbial gas, and then filled the M-reservoir in NFB and EFB from spilling around fault tips. When the buoyancy of hydrocarbon exceeded the

capillary restraining pressure of the overlying shale, the hydrocarbon leaked into the structurally higher CFB of the upper J-reservoir, then backfilled the J sands in NFB and EFB. The NFB and EFB also received limited separate oil charge leaked directly from the NFB and EFB of deeper M-reservoirs, respectively. Reservoir quality in the EFB is poor (Milkov et al., 2007). As a result, the J-reservoir in CFB received the oil leakage from the top of the M-reservoir containing the first arrived oil. Therefore, in CFB, the J-reservoir has the least mature hydrocarbon (Milkov et al., 2007).

After the discovery well BP MC127#1, eight appraisal and 11 development wells (including sidetracks) penetrated the pay zones (Milkov, 2007). Hydrocarbon was produced from M-reservoir by 7 wells (A1-A5, A8 and A9) and from J-reservoir by A10. Two injector wells, A6 and A7, were drilled at the down-dip west side of NFB and the southern downdip side of CFB of M reservoir, respectively. All wells in M except A5, A8 and A9 responded to the injection. Time-lapse geochemical (TLG) data indicate that there is a flow barrier between A10 and two appraisal wells to the east in the CFB, and that there is a flow barrier between CFB and NFB (Milkov, 2007). It is likely that the J-reservoir in NFB is not drained and drilling appraisal wells in J reservoir in NFB is justifiable. Geochemical data also suggest that stratigraphic flow baffles formed by levee or overbank deposits prevented fluid mixing but allowed fluid transmission during production (Milkov, 2007).

3. METHODS AND DATA INTERPRETATION

The data set for this study was provided by BP, Inc. to Texas A&M University. There are two depth seismic volumes, one base survey and one monitor survey. A three dimensional seismic volume and well log data set was imported to reservoir analysis software PETREL^{TM} (2011) for data interpretation and modeling. The depth is controlled by over 20 wells and their side tracks.

Seismic data are quadrature data, which zero-crossing of seismic wave form indicates impedance contrast (i.e. formation top/bases; Ikelle and Amundsen, 2005). The average frequency is relatively low (~10 Hz peak frequency). Inline spacing is 22.5 m and the crossline spacing is 12.5 m. The data set also includes 18 wells with mostly triple combo logs (gamma ray log, resistivity log, neutron porosity and density log) and one well with quad combo logs (triple combo and sonic log).

3.1 Well log interpretation

3.1.1 Porosities

Raw neutron porosity shows good porosity for both J and M sand, with all clean sands exceeding ~25% porosity, with an average porosity of 36% for J sands and 30% for M2 sands (Fig. 6). Average bulk density is around 2.15g/cc for both J sands M sands. By applying the density porosity formula for sandstone formation:

$$\phi_\rho = (\rho_{ma} - \rho_b)/(\rho_{ma} - 1) \quad \text{.....(1)}$$

Where ρ_{ma} is the matrix density, which is 2.65 g/cc for sandstone, ρ_b is the measured bulk density and ϕ_ρ is the density porosity. The calculated density porosity for

both sands is around 30% from equation (1). As a conventional way to quickly estimate the effective porosity for the clean zone, the average is calculated between apparent neutron porosity and calculated density porosity. As the result, the porosity for J sand is 33% and for M2 is 30%. The observed porosity for clean sands in sidewall cores averages slightly lower than well porosity, in the range of 26-32% (28% average) for J sands and 25-31% (~27% average) for M2 sands.

3.1.2 Gamma-ray and N/G calculation

Net to Gross ratio (N/G) is likely to be the parameter with the largest variation and uncertainty in volumetric calculation. Calculation of N/G involves two major parts, the net sand and the gross interval. Net sands are defined by 3 cut-offs, porosity, permeability and shale volume (V_{sh}). Cut-off values for porosity is variable but for a sandstone to be producible, 12% is commonly used and also used for this study (Shepherd, 2008). At discussed previously, porosity for all J and M sands is >25%.

In the Horn Mountain reservoir zone, all sandstone and shaly sandstone exceed the cut off for 'Net Sand'. Permeability of the sandstone is in the range of 100-6000 mD for all of the sandstone. Since permeability is high enough to produce out of the sands, and permeability is the one of the standard measurement form the logs V_{sh} is the only controlling cut-off that was used to define 'Net Sand'.

Shale Volume (V_{sh}) is calculated using the linear equation (Asquith and Krygowski, 2004):

$$V_{sh} = I_{GR} = \frac{GR_{\log} - GR_{\min}}{GR_{\max} - GR_{\min}}$$

Where GR_{log} is the Gamma Ray readings from the log, GR_{min} is Gamma Ray for clean sands and GR max is the Gamma Ray for shale. Vsh is calculated for J and M intervals for each log. Then a 50% V_{sh} cut-off is applied to define net sands shown as yellow intervals in Figure 5 and 6.

Gross interval is normally defined as the Measured Depth (MD) from well top to well base for target reservoir intervals. Since the N/G will be used to calculate volume based on seismic interpretation, the interval between seismic tops and bases are used. (Figure 6). Interpolated seismic tops are generally within 100 feet of the well tops, and most of them are within 20 feet of the well tops due to overall adequate well control and a good velocity model.

Table 1 summarizes the calculated N/G ratio from the wells with available data. The J Sand has an average observed N/G of ~24% and the M2 Sand has an average observed N/G at ~ 43%. The 'Net' calculated here is based on the V_{sh} cut off. Since both J and M2 sands are laminated thin sands, there may be some 'skipped pay' due to inadequate Gamma Ray resolution, the true net may be slightly higher than calculated, especially for the J sands towards the top, where thin sand beds occur (Fig. 8 log insert).

Table 1 N/G Calculation for J and M Sands

Well	J Sand			M2 Sand		
	Seismic Gross Interval (ft)	Net (ft)	N/G	Seismic Gross Interval (ft)	Net (ft)	N/G
A1	340	85	0.25	188	98	0.52
A2	208	75	0.36	202	79	0.39
A3	249	97	0.39	246	191	0.78
A4	264	103	0.39	422	159	0.38
A5	367	49	0.13	366	134	0.37
A7	358	86	0.24	323	133	0.41
A8	242	81	0.33	241	61	0.25
A9	574	81	0.14	553	225	0.41
A10	359	51	0.14	N/A	N/A	N/G
126-1st2	486	42	0.09	323	148	0.46
126-5	614	110	0.18	258	122	0.47
126-5st1	N/A	N/A	N/A	277	86	0.31
127-1st1	244	51	0.21	175	92	0.53
127-1st2	454	72	0.16	500	166	0.33
127-2	200	50	0.25	N/A	N/A	N/G
127-2st1	200	50	0.25	N/A	N/A	N/G
127-2st2	543	160	0.29	432	167	0.39
Average	356	78	0.24	322	133	0.44

3.2 Seismic interpretation

3.2.1 Horizon Interpretation

The three sand packages (J, K and M) are all low impedance sand units. Based on the quadrature seismic volume, the J and M2 top and base were mapped at the zero-crossing above and below the trough (Fig. 7). The sufficient well control and good velocity model, most wells show very good correlation between seismic tops and well tops within 20' (Fig. 6). Since all sands (J, M1, M2 and M3) are low impedance sands,

the zero-crossing generally picks the top of the sands, but locally, individual sand within M (M1, M2 and M3) cannot be resolved when two sands amalgamate. Four horizons were interpreted: J Top, J Base, M2 Top and M2 Base, throughout the seismic volume.

3.2.2 Fault interpretation

Faults were picked along seismic inlines and crosslines, using the PETREL™ Ant Tracking work flow that was designed to help fault picking by identifying local reflector discontinuity. Due to seismic quality limitations, it is generally not very helpful in fault tracking because the relative low seismic resolution. Most of the faults in the seismic volume are normal and steeply dipping. The traps are supported by salt canopy below and an extensional region above the crest. The Horn Mountain field is characterized by a series of NW-SE trending normal faults.

The fault throw increase from east to west to over 3000 ft (Fig. 7). The trap is to the south of the fault on the foot wall (high side). The structural high is a salt supported structure. The field is further divided by a west-east trending north-dipping fault (F2) and a north-south trending, west dipping fault (F3) into NFB, EFB and CFB (Fig.7).

3.3 Seismic and log characters and interpretation of depositional environment

Characters of J sands clearly show channel geometries characterized by lenticular-shaped, discontinuous reflectors and gull-wing profiles in a seismic cross-section (see Fig. 8), which indicates mud-filled channels and levees (Beaubouef and Friedmann, 2000, Sprague et al., 2005). Gull-wing shaped reflectors of J sands suggest a

leveed channel complexes with abandoned channel filled with mud. The sediments are interpreted to be deposited by overbank deposition of low concentration turbidity flows and contain low to moderate sand percentages, resulting in a low Net to Gross (N/G) value (Fig. 8). The leveed channel complex also is indicated in the well log by a fining upwards sequence (Fig. 8).

An RMS (Root Mean Square) extraction map for the J and M2 sands (Fig.10) shows elongate channel geometries as indicated by red arrows. Minimum Amplitude maps (Fig. 16) shows a similar sand pattern. The J sand fairway is oriented north to south, whereas M2 sands are oriented northwest to southeast. The low amplitude for J sands towards the west indicates lack of reservoir presence there, whereas M2 sands have oil charged reservoirs to the northwest (Well 126-5).

The RMS extraction map shows elongate high amplitude geo-bodies with gull-wing geometries (Fig. 8), so J sands are interpreted to be more confined than M2 sands. In an environment of deposition (EOD) scheme defined by Sprague et al. (2005; also illustrated by Kendall, C at http://sepmstrata.org), J is interpreted to be a leveed channel complex in a slope setting (Fig.10), which is characterized by lower N/G ratio and overall thin bedded sands (insert in Fig. 8). M2 was likely deposited more basinwards as distributary channel complexes, with higher N/G ratio and less laminated sands. The well logs show an overall fining upwards pattern. J sands have an average N/G around 25% and M2 have an average N/G around 45% (Fig. 11).

As discussed for EOD, J is likely a confined channel complex (CCC) or Leveed Channel complex (LCC) and M2 is likely to be a weakly confined channel complex

(WCCC). Stacking of the channel complex makes a Channel Complex Set and stacking of Channel Complex Sets makes composite sequences. J and M2 sands in the log are part of the composite sequence. Also they tend to have overall different N/G from each other due to different EOD, they do have similar lateral facies variation, from channel axis, to channel off-axis, to channel margin and channel fringe, each with decreasing N/G. Core data and core photos show a lateral and vertical variation from sandy channel axis, to laminated off-axis facies to muddy distal/fringe facies (Fig. 8).

3.4 Seismic amplitude attributes and the correlation with N/G ratio

Under certain conditions, seismic data allow us to infer geological information such as fluid content, abnormal pressure/temperature, and lateral variation in porosity, lithology or thickness (Chambers and Yarus, 2002). Since the sands are low impedance compared with sale, for a sand body, increasing sand content would result in decreasing seismic impedance and increasing magnitude of seismic trough at a sale/sand interface. Similar to sands from Marlin oil field, Brazil off shore, the sands in Horn Mountain is low impedance sands. Wedge model shows that at or below tuning thickness, due to the interference between seismic response of top and base reservoir, negative amplitude is stronger when reservoir sand gets thicker (Rildo et al. 2005). An attempt was made to quantify the correlation of seismic amplitude and net sand thickness and reservoir N/G, which shows similar relations.

By applying a 50% V_{sh} cut-off, with considerable scatter, RMS amplitude shows a weak positive correlation with N/G ratio from the investigated interval (Fig. 11).

Correlations between seismic attributes and reservoir characters such as N/G ratio were discussed by numerous authors (Hanna et al., 1991; Connolly et al., 2002; Vernik et al., 2002; Rildo et al., 2005). A positive correlation occurs for a reservoir of low impedance sands below tuning thickness and a flattened amplitude at higher net thickness (Rildo M. et al. 2005). Since the reservoir gross thickness is relatively uniform at 200-250 ft thick (isochore) for M and J sands, the N/G is proportional to net thickness. Reservoir sands generally have net thickness below tuning thickness and there is positive correlation of amplitude with N/G. However, the amplitude flattens out with increasing net thickness beyond tuning thickness. This observation is especially true for M2 sands where the N/G is relatively high so the net thickness is much higher than the tuning thickness. Based on these observations, the tuning thickness for the seismic volume is at about 0.4 N/G for M2. Since the gross interval is about 250 ft, the tuning thickness for the volume is about 250*0.4=100 ft.

It appears that amplitude strength is also effected by hydrocarbon effect (i.e., oil sands tends to have lower impedance) which results in higher amplitude, where sands above the oil water contact have distinctively higher RMS amplitude strength and amplitude is confined very well to structure (Fig. 9). As the result, amplitude strength is a combination of N/G and hydrocarbon fluid effects, where hydrocarbon distribution is probably a significant control, due to the scattering between N/G and the strong correlation between the fluid contact and amplitude distribution (Figs. 9 and11).

As a result of the analysis, it is not practical to apply a linear equation to estimate N/G based on amplitude strength of the seismic signal. The approach here is to apply a representative N/G to high, and low amplitude zones for volumetric calculation.

3.5 Fluid distribution and its implication for trapping style and charging history in this reservoir

The oil water contact (OWC) for J sand occurs at 13,022 ft TVDSS at A3 in NFB and from M2 Sands from Well A7 at ~ 14,340 ft TVDSS in CFB (Fig. 12). This is consistent with flat spots observed in seismic data (Fig. 11). The primary gas cap might occur here but it is a relatively small chance since no gas is observed from any of the J and M2 penetrations. The 13,022 ft TVDSS OWC for NFB is consistent with an abrupt amplitude termination (flat spot) at this level (Fig.12 and 13). Since the amplitude is fit to structure, it is very likely that CFB has an OWC at around 12,890 ft TVDSS where indicated by the amplitude distribution (RMS and Minimum Amplitude). The observed highest known water at A7 is 13,100 ft TVDSS and the OWC is about 12,890 ft TVDSS at A5. The observed MDT data shows the gradient and fluid contact is consistent with observations.

For J sands, all the wells east of A3 in NFB and CFB penetrated to in the oil leg above the oil water contact, and the J sands in A3 are wet. A9 which penetrated J sands in EFB is wet, indicating no communication between CFB and EFB at a geological time scale via sand juxtaposition below the highest known water in A9 (Fig 13). Since source abundance is rarely a risk in the Gulf of Mexico, hydrocarbon migration is the main

constraining factor for hydrocarbon distribution here. Since the J sand in EFB is wet with its highest known water at ~12,486 ft TVDSS that indicates the NWF and CFB likely were charged directly from underlying sediments and then flowed to the EFB.

Since high-amplitude signatures are confined very well to structure in NFB and CFB, EFB is likely to have the same amplitude indicator for hydrocarbon contact. The abrupt amplitude change occurs at around 12,200 ft TVDSS and the amplitude change is confined to structure (Fig. 14). This overall migration history is consistent with what is indicated geochemistry data.

Fault throw for both Faults 2 and 3 are relatively small. Fault 2 has maximum throw of 200-250 ft which is close to the thickness of J sands, which is around 250 feet. Fault plane profile along fault 2 shows significant sand juxtaposition (Fig. 14), which indicates it is leaking hydrocarbon. However, J sands in NFB and CFB have different OWC's, indicating sealing faults between these blocks (Fig. 14). The sealing capacity of faults in hydrocarbon migration has long been a topic of controversy (e.g. Jones and Hillis, 2003; Knipe, 1997; Knipe et al., 1998; Yielding et al., 1997). In fact, the fault seal capacity is not only a function of fault plane gouge and its mechanical properties but it also is a function of timing. Faults are very risky as a seal because in a geological time scale, sand on sand juxtaposition is always vulnerable to leaking; however, in a production time scale, faults are almost always a barrier, or a production compartment boundary (Jones and Hillis, 2003). At Horn Mountain, different OWC of J sands in all three fault blocks implies that the faults are impermeable to hydrocarbon migration. However, the close juxtaposition of J sands across faults and the same water gradient

trends across fault (Fig 14 insert) suggest that this is likely to be a system that has not reached long term equilibrium (i.e., it is still actively charging either from M sands beneath or/and across the faults from the J of NFB). Different OWC's for all 3 fault blocks is a function of different charging rate, container size of different block and any potential leakage.

For M2 sands, A7 which penetrated the OWC at ~ 14340 ft TVDSS. Unlike J1, M2 has a uniform OWC and M2 is hydrocarbon bearing at EFB. This implies that the EFB was charged through sand juxtaposition from CFB with its higher seal capacity.

The overall charging history is the model proposed by Milkov et al. (2007) with some differences in later stages (Fig. 15). After charging with microbial gas followed by charging M reservoir from CFB as indicated oil maturity gradient in different fault blocks. In Milkov's model, J sands ware charged from CFB then NFB and EFB. This model cannot explain how K sands could be bypassed by vertical oil migration. Also, lower OWC in NFB cannot be adequately explained if it is charged from CFB. Based on these observations, this study proposes that the sequence of hydrocarbon charging as the following steps: 1. prior to oil migration, all M, J and K sands are filled with microbial gas; 2. Hydrocarbon from source rock (probably Jurassic and Cretaceous source) migrated up along fault 1; 3. M sands in NFB first, then CFB and EFB, from north to south; 4. J sands in NFB were charged, then CFB and EFB, from nor to south; 5. K sands were bypassed due to no access to F migration conduit (Fig. 15). J sands are likely to have stratigraphic boundaries or structural baffles so it has multiple OWCs, whereas

M2 sands are more connected (distributary system). F2 and F3 sands are unlikely to be flow barriers but may be baffled.

Both J and M sand structures have a saddle to the west and a high side 3 way closure against Fault 1 (Figs. 12 and 13). The overall trap for J and M2 sands on NFB is a faulted stratigraphic trap, with sand pinch-out to the east. M2 OWC could be controlled by sand juxtaposition along F1. If this is the case, the exit point through F1 is likely to be deeper than the saddle point (pointed by the red arrow in Fig 13). This is confirmed by the presence of hydrocarbon charged reservoir in the smaller NW high side 3-way trap. This trap does not have stacked J and M pay, because it is outside of the J channel fairway which is more confined than the fairway M, therefore J sand is not present here.

4. VOLUMETRIC CALCULATION

4.1 Environment of deposition mapping

Environment of deposition (EOD) was mapped based on seismic amplitude attribute and well log data. As discussed before, although there is a positive relationship between N/G and amplitude magnitude (strength), the correlation is not linear (Fig.11). Seismic amplitude strength is likely controlled by N/G and fluid type, and other factors such as reservoir thickness and processing algorithm, where only N/G is directly linked to EOD.

EOD maps were generated in to honor observations from both seismic data and well log data and interpretation of channel geometry based on cores and well log interpretation. Two methods are used to map EOD. The first approach was to use seismic amplitude to constrain channel facies with N/G from well logs to constrain the amplitude cut-off. The second approach is more interpretative and to honors the channel geometry with constraints from both seismic amplitude and well logs. Due to limited seismic quality, three main EOD's were mapped in both J and M2 sands: channel axis, channel off axis and channel margin.

4.2 Reservoir parameters and deterministic volumetric calculation

Stock Tank Oil Initially In Place (STOIIP) was calculated using the equation

$$STOOIP = GRV*N/G*\phi*S_w*1/B_o$$

Where GRV is gross hydrocarbon bearing rock volume, N/G is net to gross value, ϕ is the porosity, S_w is the water saturation, and B_o is the formation volume factor. GRV is determined based on the seismic interpretation where PETREL^{TM} calculates the volume between J top and J base, and volume between M2 top and M2 base. The OWC is 13,022 ft TVDSS for J sands in NFB, 12,890 ft TVDSS for J sanlds in CFB and is 12,200 ft TVDSS for EFB. The OWC for M2 sands is 14,340 ft TVDSS.

N/G is determined based on well log calibration with EOD, which is calibrated to amplitude strength. Figure 14 shows the EOD map for J and M sands. Due to the limited seismic quality and the fair N/G to amplitude strength calibration, only three facies were calculated, channel axis, channel off axis and channel margin.

Porosity is determined from logs and cores. For J sand, an average 28% is used and for M2 sands, 29% porosity is used. Water saturation of 25% for the oil zone is used from well log and production data. Formation volume factor was determined from the production data, where 1.57 is for J sands and 1.38 is for M sands. All parameters are summarized as Table 2.

Table 2 Reservoir Parameters Used for Volumetric Calculation

Base Case	OWC (ft TVDSS)			FVF	ϕ	Sw	N/G			Recovery Factor
	NFB	CFB	EFB				Channel Axis	Channel off axis	Channel Margin	
J sand	13022	12890	12200	1.57	0.29	0.25	0.35	0.15	0	0.6
M2 Sands	14340	14340	14340	1.38	0.28	0.25	0.5	0.3	0	0.6

Based on the model and all the parameters, STOIIP and recoverable resource (reserves) were calculated (Table 3).

Table 3 Deterministic Volume Calculation for hydrocarbon for J and M sands

	Resource (MBOE)	NFB	CFB	EFB	Channel Axis	Channel Offaxis	Channel Margin	Total Volume (MBOE)
J Sand	STOIIP	23	13	7	25	18	0	**43**
	Recoverable	14	8	4	15	11	0	**26**
M2 Sand	STOIIP	111	65	37	139	74	0	**213**
	Recoverable	66	39	22	83	44	0	**127**

STOIIP for J sand is 43 MOBE (Million Oil Barrels Equivalent) and for M2 sands is 312 MOBE, were recoverable oil is 26 MBOE for J sands and 127 for M2 sands.

Over half of the J sand reserve and ~2/3 of the M2 sand reserve are in the channel axis facies where the N/G is highest. Over half of the reserve for both J sands and M2 sands are in NFB, and CFB contains about 30% of the reserves for both M and J sands. EFB contains the least amount of reserves. However, 22 MOBE in M2 sands is only penetrated by oil producer A9 very close to the OWC and the 4 MOBE in J has not been tested or drained by any exploration or production wells. Since 93 MOBE was produced as of 2007, there were about 50 MOBE remaining resources. Besides increasing the recovery factor by secondary to tertiary lift aid by water injection, drilling appraisal wells and producers targeting the up-dip EFB, which contains about 28 MOBE of the remaining resource could be useful.

4.3 Uncertainties and remaining resources

The static geologic model resulted in better understanding of fluid distribution and deterministic volume calculations for different compartments. Although the Horn Mountain field is a relatively mature field with 10 exploration wells and 16 production wells and sidetracks drilled, there still are uncertainties in the volume calculation and hydrocarbon distribution. Uncertainties occur in all of the parameters in Table 2. Some of the parameters are relatively well understood and constrained, such as porosity and water saturation from the exploration and production wells. Also the fluid contact and fluid distribution is well understood for the NFB and EFB. The wells indicate seismic depth uncertainty is minimum due to moderately dense well control in the field. However, other reservoir parameters play the most important role in increasing the uncertainties of the final volumes.

The N/G distribution is determined by seismic amplitude. In a field scale, seismic amplitude is probably the only practical way to constrain facies/EODs when calibrated to well log N/G. However, the seismic amplitude is effected by so many other factors other than the sand percentage, such as fluid type and overlaying lithology, that this calibration is not as robust as desired. Another factor is the heterogeneity of N/G distribution, where averaged N/G was used to represent the highly variable sand distribution in a deepwater channel system.

Recovery factor (RF) is another major uncertainty in this analysis. Since RF is a function of reservoir quality, connectivity, permeability, finer scale stratigraphic and structural compartmentalization, which the seismic data does not further constrain. It is

also constrained by reservoir driving mechanisms and completion methods/technologies. A reservoir simulation dynamic model is necessary to history match and future constrain the uncertainties, but it is beyond the scope of the static model determined here.

Another uncertainty comes with the primary gas-occupied volumes. Although the gas cap is thought to be relatively small and no gas was penetrated in logs, gas cap is likely to present in both J and M reservoirs. Gas or gas condensate is not counted for this model due to the lack of Gas Oil Contact (GOC) information.

M sands consist of three channel complexes M1, M2 and M3, but since the volume contribution from M1 and M3 sands is not significant, they are not considered for the model. M1 and M3 sands are not continuous and the sands are only locally present, a geobody analysis would be necessary to determine the hydrocarbon volumes, distributions and connectivity within these channelized sands.

4.4 Recommendations for future work

Production at Horn Mountain has shown a marked decline since 2006 with increased water cut in some production wells (Wood Mackenzie data base). This decline will continue until some mid-life well rework is performed. Based on the economics, in addition to well work to boost production from the existing producers, it is worth looking into the up-dip portion of EFB for additional resources.

5. CONCLUSIONS

Horn Mountain Field was discovered in 1999 and had produced its first oil in 2002. The production is from Middle Miocene J and M sands. J sands were deposited in a relatively confined levee channel with lower N/G (~15-40%) and M sands formed a confined channel with higher N/G (20-80%).

This study characterized the reservoir by utilizing the available core, wireline log and seismic data to identify the remaining development opportunities. The field is divided into three fault blocks (NFB, CFB and EFB) by a series of faults. The faults appear to be sealing with sand juxtaposition for J sands, which indicate a relatively recent charge or active charge for the J reservoir. The total deterministic volume calculated from modeling is 26 MOBE for J sands and 127 for M2 sands, which is the main contributor from stacked M sands. Over half of the reserves for both J and M sands are within NFB, and around 30% in CFB. Only one well produced the down-dip portion of M2 from the EFB. There is potentially 4 MOBE from J and 22 MOBE recoverable from M2 in EFB, where the 4 MOBE of J sands was not penetrated tested or produced.

REFERENCES

Asquith, G. and Krygowski, D., 2004. Basic Well Log Analysis: AAPG Methods in Exploration 16, p. 31-35.

Beaubouef, R.T. and Friedmann, S.J., 2000. High Resolution Seismic/Sequence Stratigraphic Framework for the Evolution of Pleistocene Intra-Slope Basins, Western Gulf of Mexico: Depositional Models and Reservoir Analogs, Deep-Water Reservoirs of the World, Gulf Coast SEPM Foundation, 20th Annual Bob F. Perkins Research Conference, Deep-Water Reservoirs of the World, p. 40 – 60.

BP Management Review, 2008. Data and interpretation provided by BP Inc. geologists to Texas A&M University.

Bramlett, K. and Kendrick, J., 2000. NOGS: Gulf of Mexico Deepwater Forum, Short Course #1, Am. Association Petroleum Geologists Annual Convention, April 16-19, 2000, New Orleans, LA.

Chambers, R.L. and Yarus, J.M., 2002. Quantitative use of seismic for reservoir characterization. CSEG Recorder, 14-25.

Kendall, C. G. St.C., SEPM Stratigraphy Web and the references therein http://www.sepmstrata.org/.

Clemenceau, G.R. and Miller, P.L., 1993. Fanlobe geometry and reservoir sand characteristics of Ram/Powell Field, Deepwater Gulf of Mexico: 68th SPE Annual conference, Houston, Texas, paper SPE26441, p. 261-262.

Clemenceau, G.R., Colbert, J., and Edens, D., 2000. Production result from Levee-Overbank Turbidite Sands at Ram/Powell Field, Deepwater Gulf of Mexico, GCSSEPM Foundation 20th Annual Research Conference Deep-Water Reservoirs of the World, December 3-6, 2000, p. 15.

Connolly, P.A., Schurter, G., Davenport, M., and Smith, S., 2002. Estimating net pay for deep-water turbidite channels offshore Angola; 64th EAGE Conference & Exhibition, Extended Abstracts, G-28.

Continental Shelf Associates, Inc. 200. Deepwater Gulf of Mexico Environmental and Socioeconomic Data Search and Literature Synthesis. Volume I: Narrative Report. U.S. Department of the Interior, Minerals Management Service, Gulf of Mexico OCS Region, New Orleans, LA. OCS Study MMS 200-049, 340 p, p. 26-28.

Doughty, P.T., 2003. Clay smear seals and fault sealing potential of an exhumed growth fault, Rio Grande rift, New Mexico: AAPG Bulletin, v.87, p. 427-444.

Hanna, R., Reynolds, D., Horkowitz, J., and Dillon, W., 1991. Integrated Method for PAYTHICK Calibration in Plio-Pleistocene Slope Sediments, Offshore Texas, Gulf of Mexico, AAPG Bulletin, v.75, p. 589 – 589.

Hood, K. C., Wenger, L. M., Gross, O. P., and Harrison, S. C., 2002. Hydrocarbon systems analysis of the northern Gulf of Mexico: Delineation of hydrocarbon migration pathways using seeps and seismic imaging, in Surface exploration case histories: Applications of geochemistry, magnetics, and remote sensing, D.

Schumacher and L. A. LeSchack, eds., AAPG Studies in Geology No. 48 and SEG Geophysical References Series No. 11, p.25–40.

Ikelle, L. and Amundsen, L., 2005. Introduction to Petroleum Seismology (Investigations in Geophysics No.12), Page 173-175.

Jones, R. M. and Hillis, R. R., 2003. An integrated, quantitative approach to assessing fault seal risk: AAPG Bulletin, v. 87, p. 507-524.

Kendrick, J., 2000. Turbidite Reservoir Architecture in the Northern Gulf of Mexico Deepwater: Insights from the Development of Auger, Tahoe, and Ram/Powell Fields. *In:* Weimer P., et al. *(eds)* Deep-Water Reservoirs of the World, Proceedings of the GCSSEPM Foundation 20th Annual Research Conference, The Write Enterprise, Houston, Texas, p. 450–468.

Knipe, R. J., 1997. Juxtaposition and seal diagrams to help analyze fault seals in hydrocarbon reservoirs: AAPG Bulletin, v. 81, p. 187–195.

Knipe, R. J., Jones, G., and Fisher, Q. J., 1998. Faulting, fault sealing and fluid flow in hydrocarbon reservoirs: an introduction. In: Jones, G. and Fisher, Q. J. and Knipe, R. J. (eds) Faulting, Fault Sealing and Fluid Flow in Hydro-carbon Reservoirs. Geological Society, London, Special Publications 147, p. vii-xxi.

Little, A.D, 2013. Deepwater Developments, Critical Aspects and Key Considerations for Technology Selection, p.1.

McDonnell, A., Loucks, R.G., and Galloway, W.E., 2008. Paleocene to Eocene deep-water slope canyons, western Gulf of Mexico: Further insights for the

provenance of deep-water offshore Wilcox Group plays, AAPG Bulletin v. 92, p. 1169-1189.

Milkov, A.V., Goebel, E., Dzou, L., Fisher, D.A., Kutch, A., McCaslin, N., and Bergman, D.F., 2007. Compartmentalization and time-lapse geochemical reservoir surveillance of the Horn Mountain oil field, deep-water Gulf of Mexico. AAPG Bulletin v. 91, p. 847-876.

OCS Report, MMS2009, Deepwater Gulf of Mexico 2009: Interim Report of 2008 highlights, p. 47.

Pfeiffer, D.S., Mitchell, B.T., and Yevi, G.Y., 2000. Mensa, Mississippi Canyon Block 731 Field, Gulf of Mexico – An integrated Field Study, GCSSEPM Foundation 29th Annual Research Conference, Deep-water Reservoirs of the World, December 3-6, 2000, p. 46.

Oliveira, R.M., Ribeiro, N.M.D.S. Jr., Johann P.R.S., Steagall, L.F.C Jr., Kerber, P.A. and Carvalho M.R.J., 2005. Using Seismic Attributes to Estimate Net Thickness in Pinch-Out Areas – Marlim Deep Water Turbidite Oilfield, Campos Basin. SPE 94913, p. 20-23.

Schlumberger online PETREL introduction, 2010. http://www.slb.com/services/software/geo/petrel/seismic/auto_structural_interpretation/ant_tracking.aspx.

Schlumberger, 2010. PETREL 2010: PETREL Introduction G&G Course, Dec 6-10, 2010, Schlumberger SIS, Houston, TX. Shepherd, M., 2009. Rock and fluid

properties, *in* M. Shepherd, Oil field production geology: AAPG Memoir 91, 1444 S. Boulder Ave. • Tulsa, OK 74119, p. 65-68.

Sprague, A.R., Garfield, T.R., Goulding, F.J., Beaubouef, T.R., Sullivan, M.D., Rossen, C., Campion, K.M., Sickafoose, D.K., Abreu, V., Schellpeper, M.E., Jensen, G.N., Jennette, D.C., Pirmez, C., Dixon, B.T., Ying, D., Ardill, J., Mohrig, D.C., Porter, M.L., Farrell, M.E., and Mellere, D., 2005. Integrated slope-channel depositional models: The key to successful prediction of reservoir presence and quality in offshore west Africa: E-Exitep, Veracruz, Mexico, Colegio de Ingenenieros Petroleros de México, p. 1-13.

Sylvester, Z., Deptuck, M.E., Prather, B.E., Pirmez, C., and O'Byrne, C., 2012. Seismic Stratigraphy of a Shelf-Edge Delta and Linked Submarine Channels in the Northeastern Gulf of Mexico: SEPM Special Publication, v. 99, p. 31-59.

Vernik, L., Fisher, D., and Bahret, S., 2002. Estimation of net-to-gross from P and S impedance in deepwater turbidites, The Leading Edge, Volume 21, Issue 4, p. 380.

Yielding, G., Freeman, B., and Needham, D. T., 1997. Quantitative fault seal prediction: AAPG Bulletin, v. 81, p. 897–917.

APPENDIX

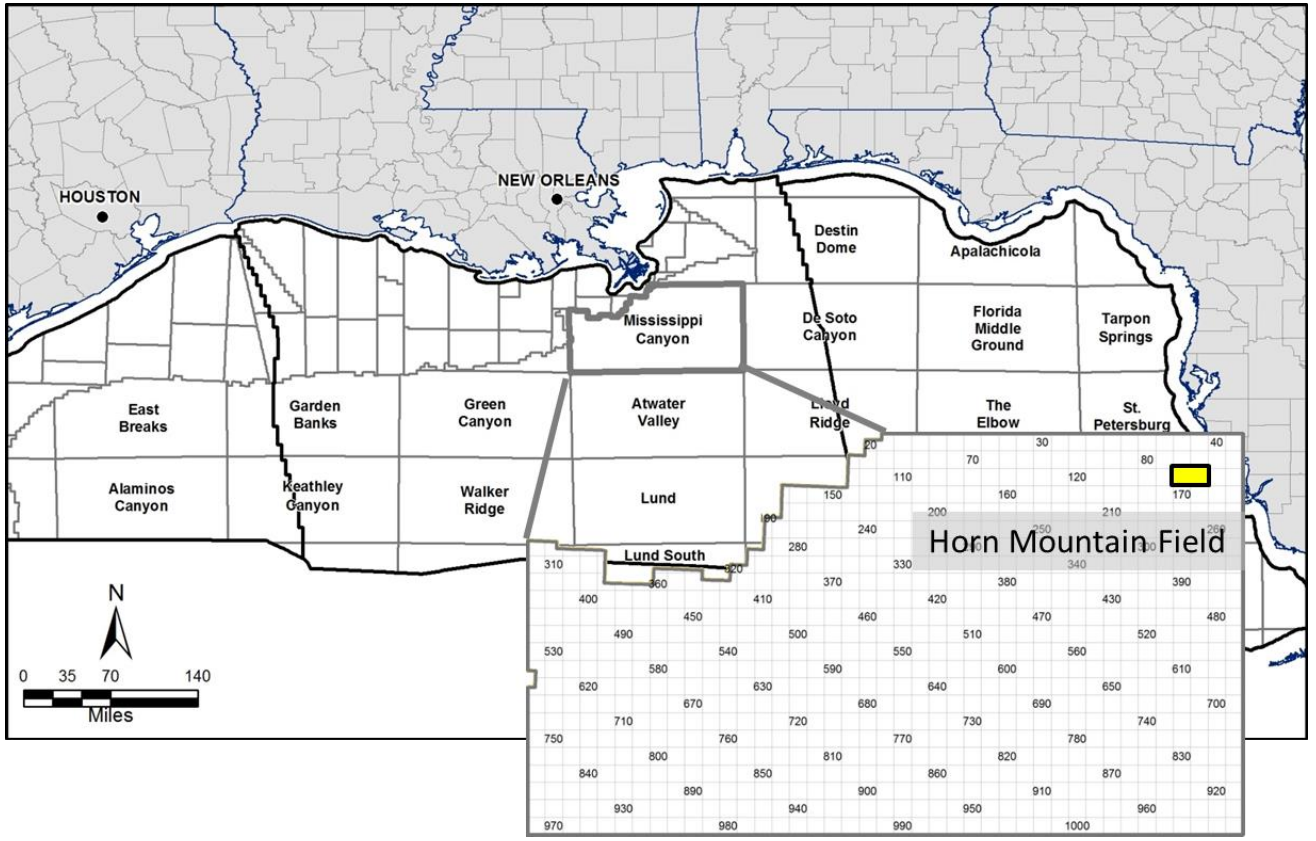

Figure 1. Location map for the Horn Mountain field, Mississippi Canyon Block 126 and 127, Gulf of Mexico; insert map shows the blocks within Mississippi Canyon Protraction Area, where the filled rectangle shows the location of Horn Mountain field).

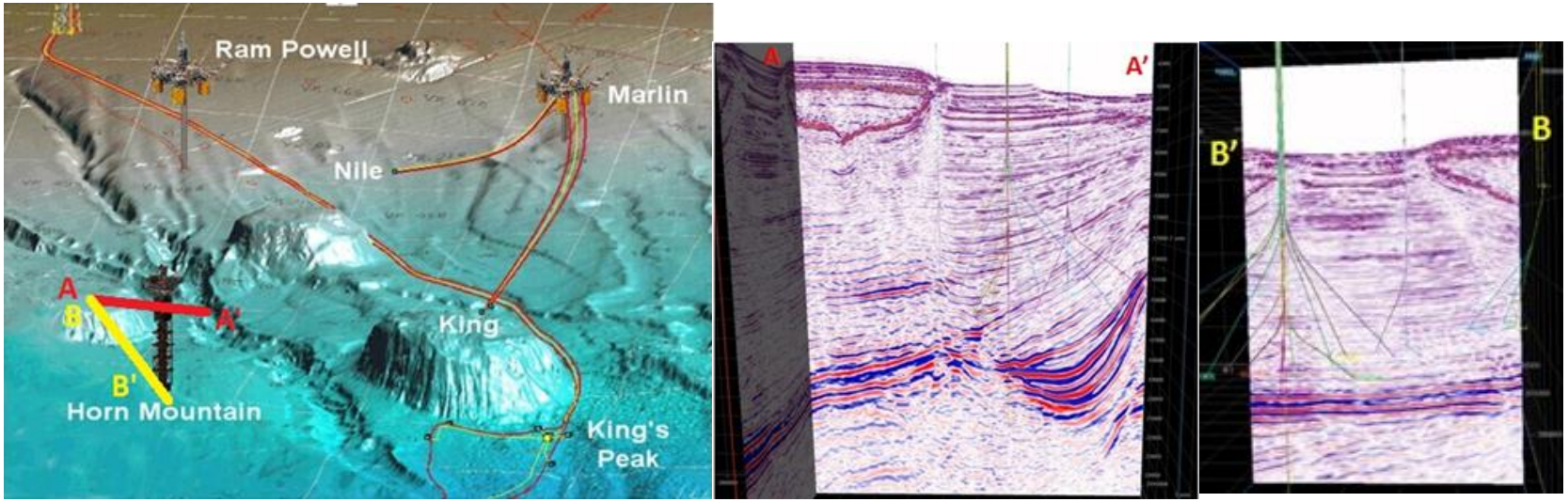

Figure 2. A) topographic map showing the location of Horn Mountain field near Mississippi Canyon. Four salt domes are recognized, two to the east of the canyon and two to the west of the canyon. Seismic line A-A' and B-B' are shown in red and yellow, respectively; B) seismic line A-A', where the northwest salt canopy, the canyon and a deep salt pillow are recognized; C) seismic line B-B', where the northwest and southwest salt dome can be recognized. The depth is from 0 to 24,000 ft (0-7315 m) subsea and the width for A is ~ 33000 ft (~10,000 m)16 and for B is ~16,500 ft (~5,000 m).

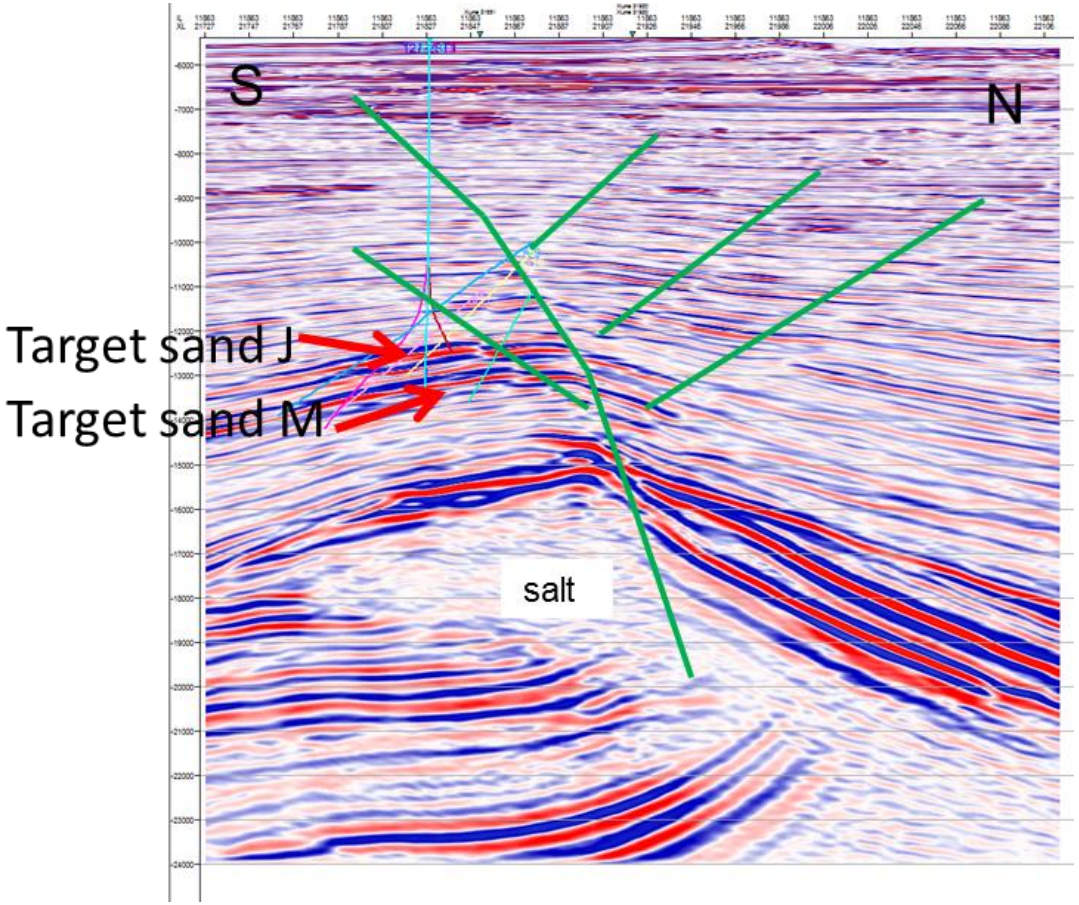

Figure 3. Seismic line (inline 11863) shows the faults developed at the crest of the salt canopy related to the emplacement of the salt diapir. Y axis is total depth subsea from 4,000 to 23,000 ft and X axis is crossline number. Green lines are interpreted faults.

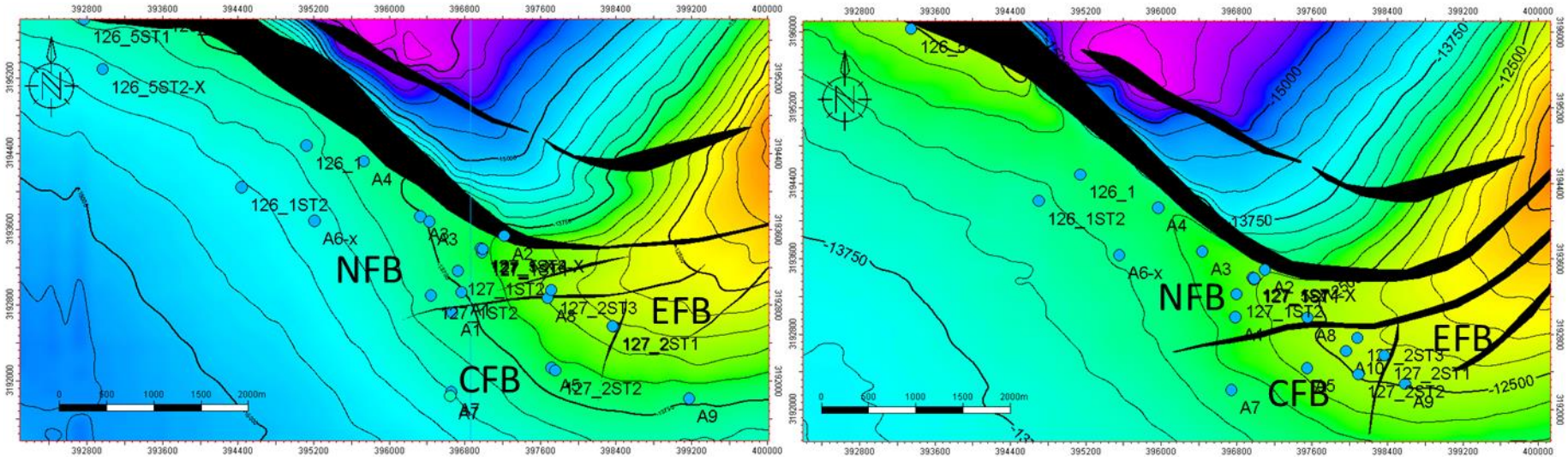

Figure 4. Depth Structure Map of A) M reservoir and B) J reservoir showing trends for regional faults (black) and the well locations and NFB (North Field Block), CFB (Central Field Block) and EFB (Eastern Field Block; Milkov et al, 2007) circles show the corresponding well tops from exploration/appraisal wells (well name starts with block numbers) and production wells (well name starts with letter 'A').

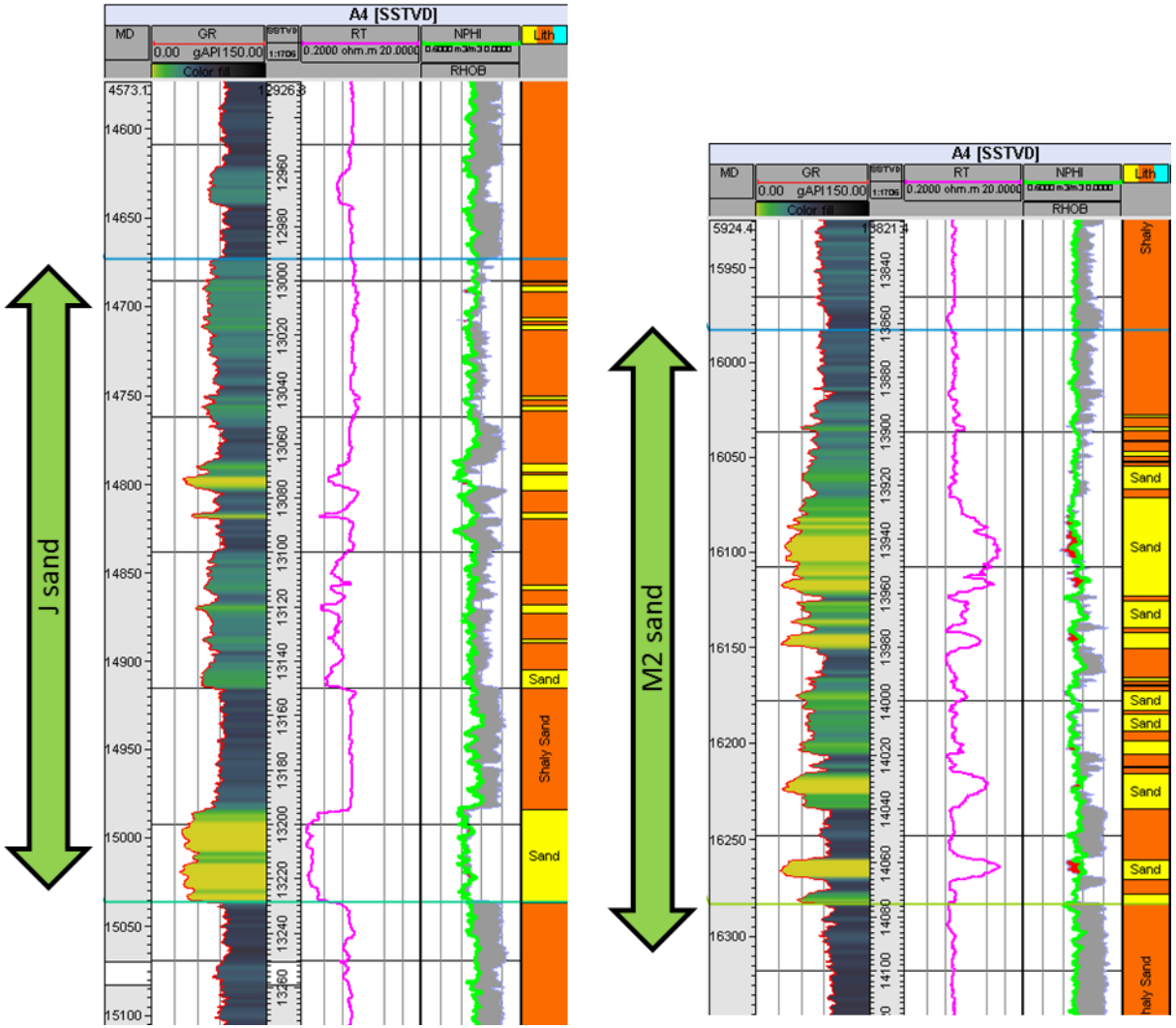

Figure 5. Triple Combo log showing typical porosity (Neutron and Density Porosity) of J and M sands; M2 sand has much higher N/G than J sand.

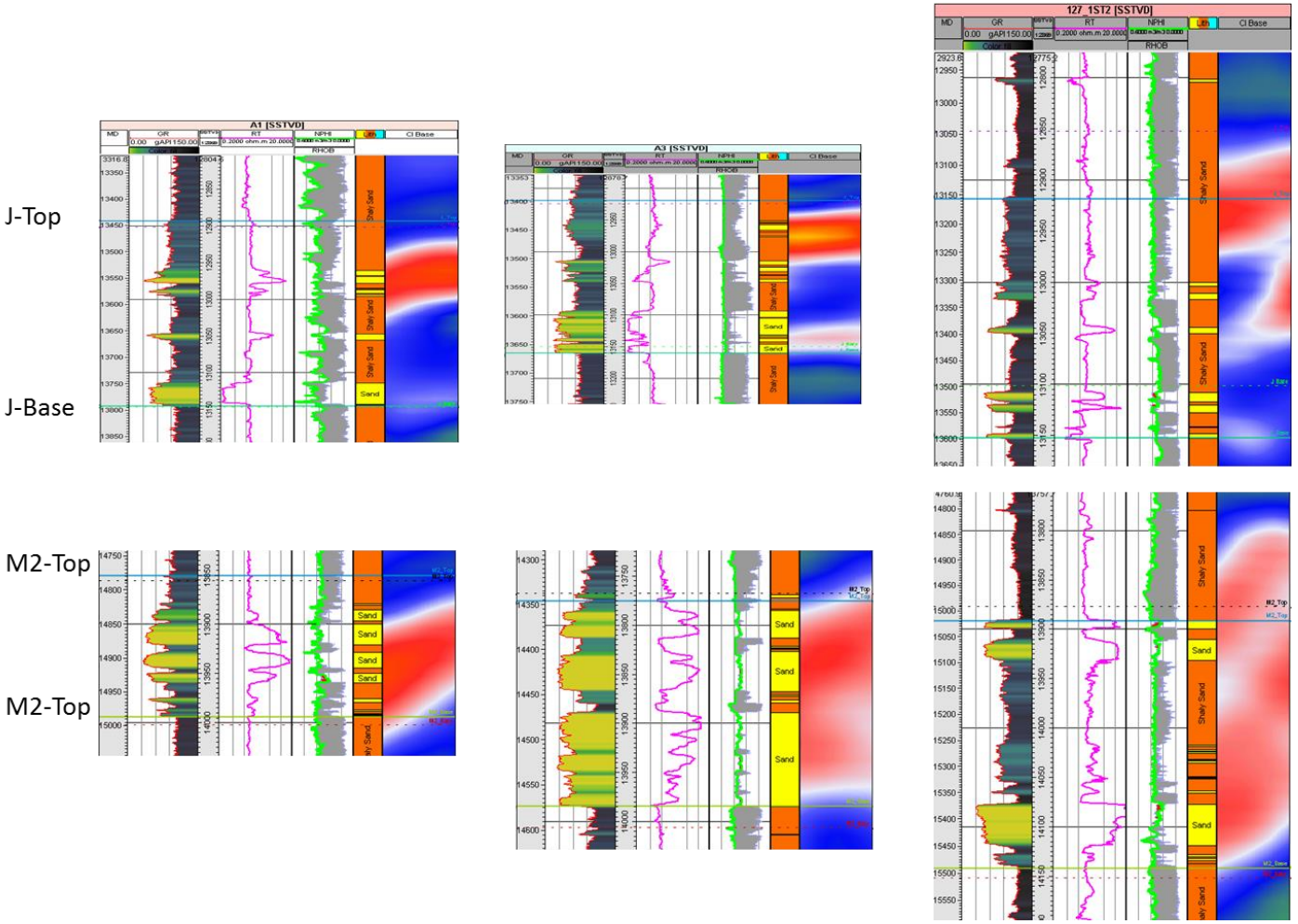

Figure 6. Triple combo well logs comparing will tops/bases and seismic tops/bases and the calculation of Net to Gross (solid lines are well tops and dotted lines are seismic interpretation), right column is quadrature seismic data where 0-crossing between positive and negative values is interpreted as shale/sand interface (red negative/blue positive); gross interval used for calculation are from interpreted seismic surfaces (between dotted lines for each interval).

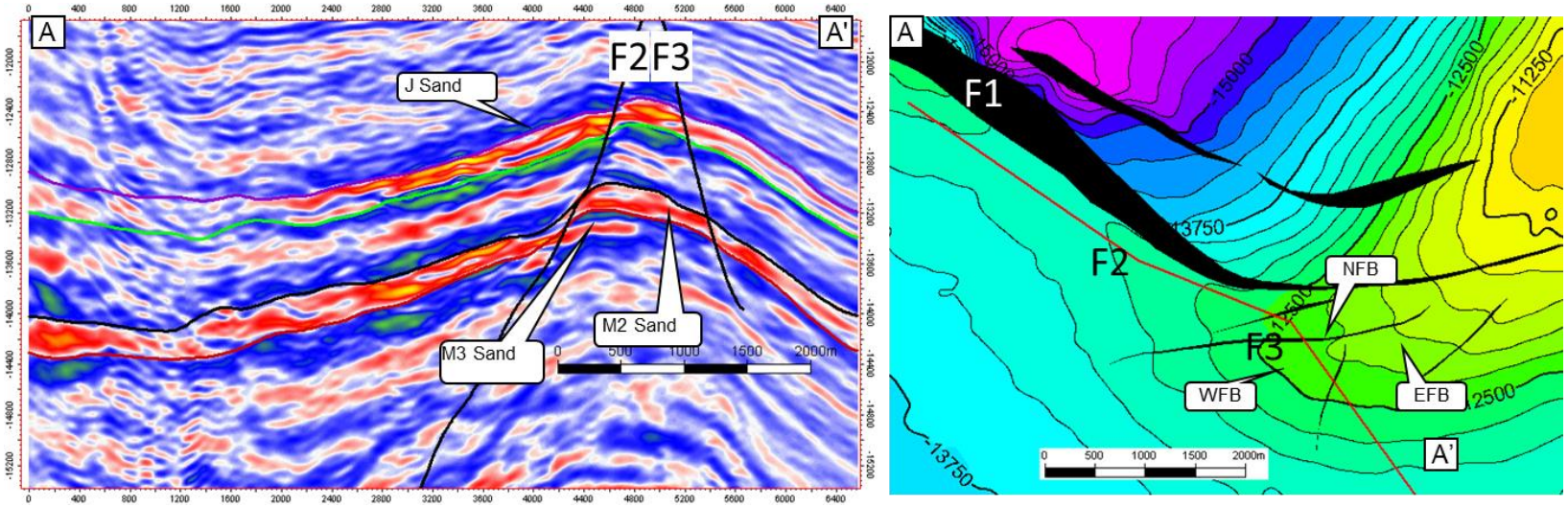

Figure 7. Seismic cross-section (A-A') shows key horizons (left) and faults with M2 Top Depth Structure Map (right).

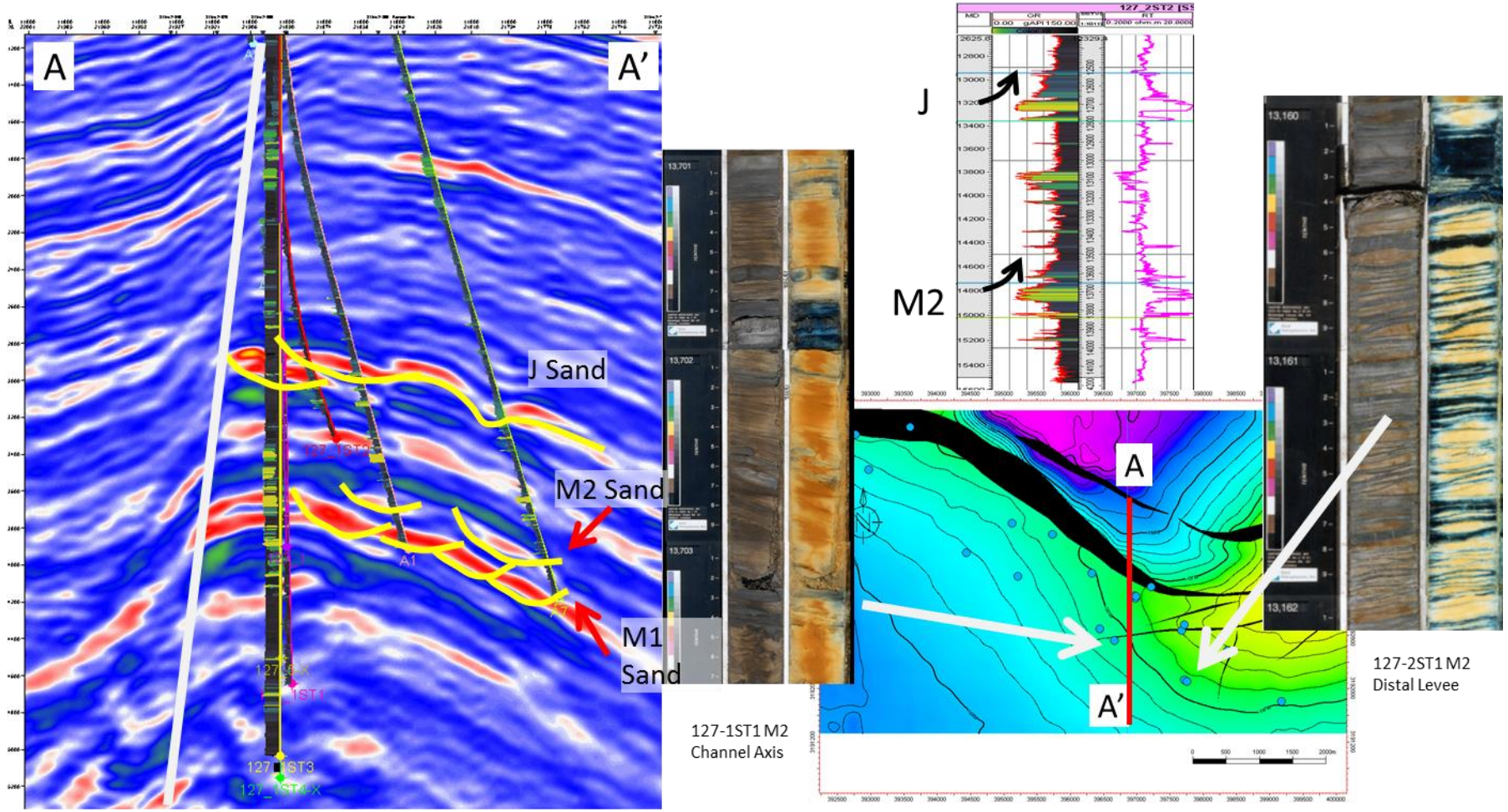

Figure 8. Cross-section (A-A') showing seismic character of J and M sands. The insert is the core image from 127-1ST1 and 127-2ST2; inserting core photos show the characteristics of sand under natural light (middle column) and ultraviolet light (right column) where sands appear to be yellow and shales appear gray to black; M2 sands have character varied from blocky channel axis sand to laminated levee sands interbedded with cm scale shale; arrows on log show a fining upward pattern.

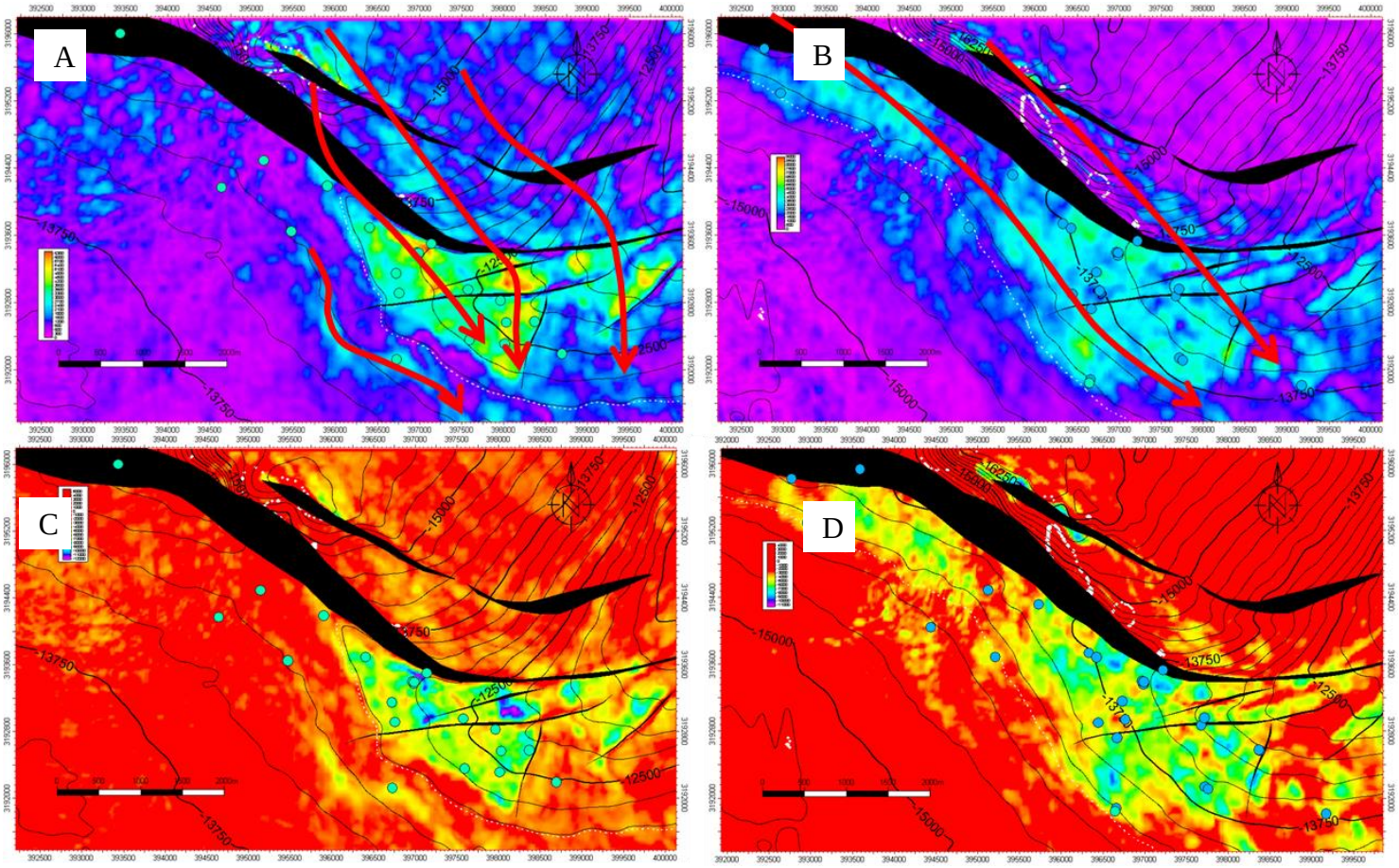

Figure 9. Root Mean Square (RMS) Amplitude extraction for a) J sands and B) M2 Sands; minimum amplitude for C) J and D) M2 sands; dotted white line indicate the Oil Water Contact from log data (Contour Interval =250 ft); red arrows shows channel fairways and flow directions for M2 and J sands; hot color indicate higher magnitude and cool color indicate lower magnitude.

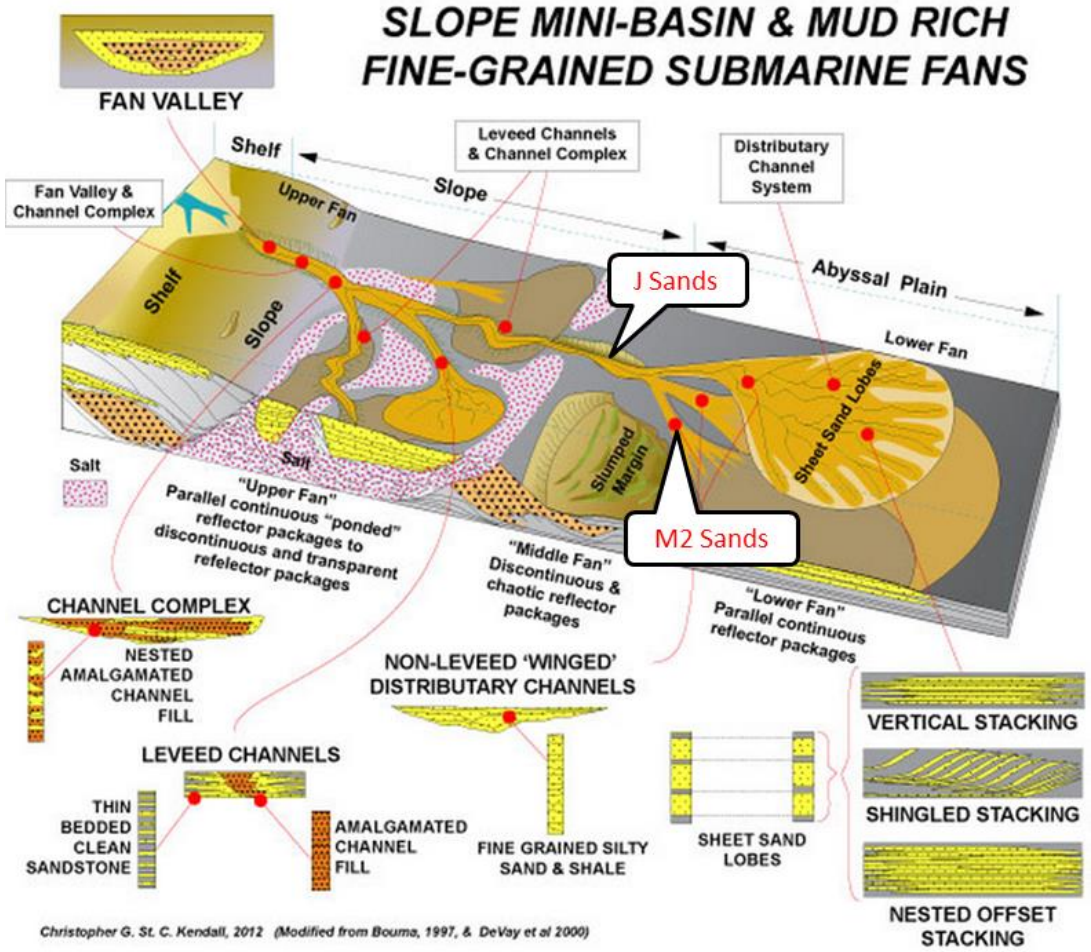

Figure 10. Deepwater environment of deposition (adapted from Christopher G. St.C. Kendall http://sepmstrata.org). J sands are interpreted to be leveed channels and M2 sands are interpreted to be weakly confined or distributary channels.

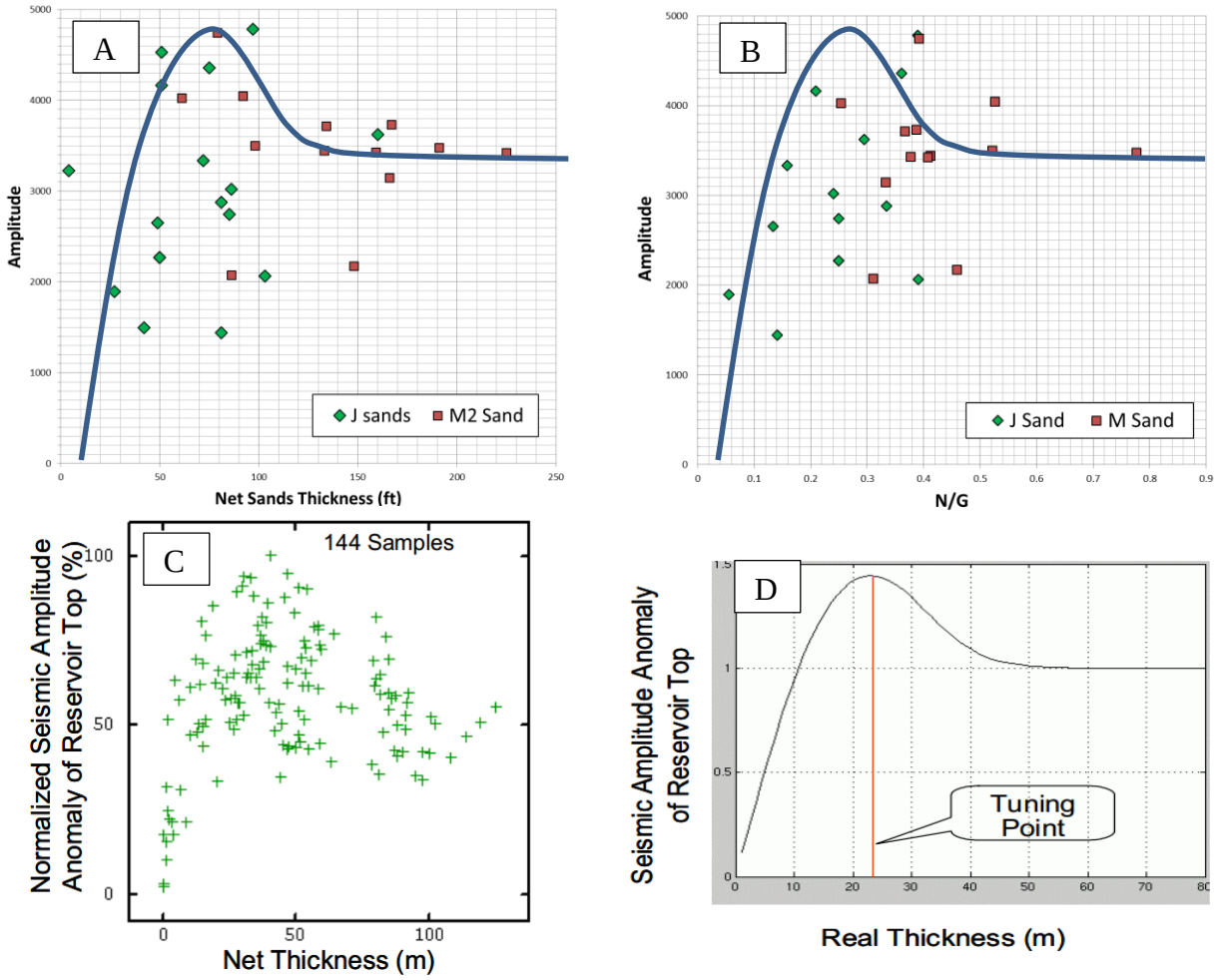

Figure 11. A) Correlation between amplitude strength and net sand thickness and B) net to gross Ratio (left; blue line is the inferred correlation); C) data from Rildo et al. (2005) showing correlation of seismic amplitude with reservoir Net thickness for real data (top right) and D) wedge (pinch-out) simulation (bottom right) below tuning thickness at around 75 ft (23 meters), where the tuning thickness observed in J and M2 sands are close to 80 ft.

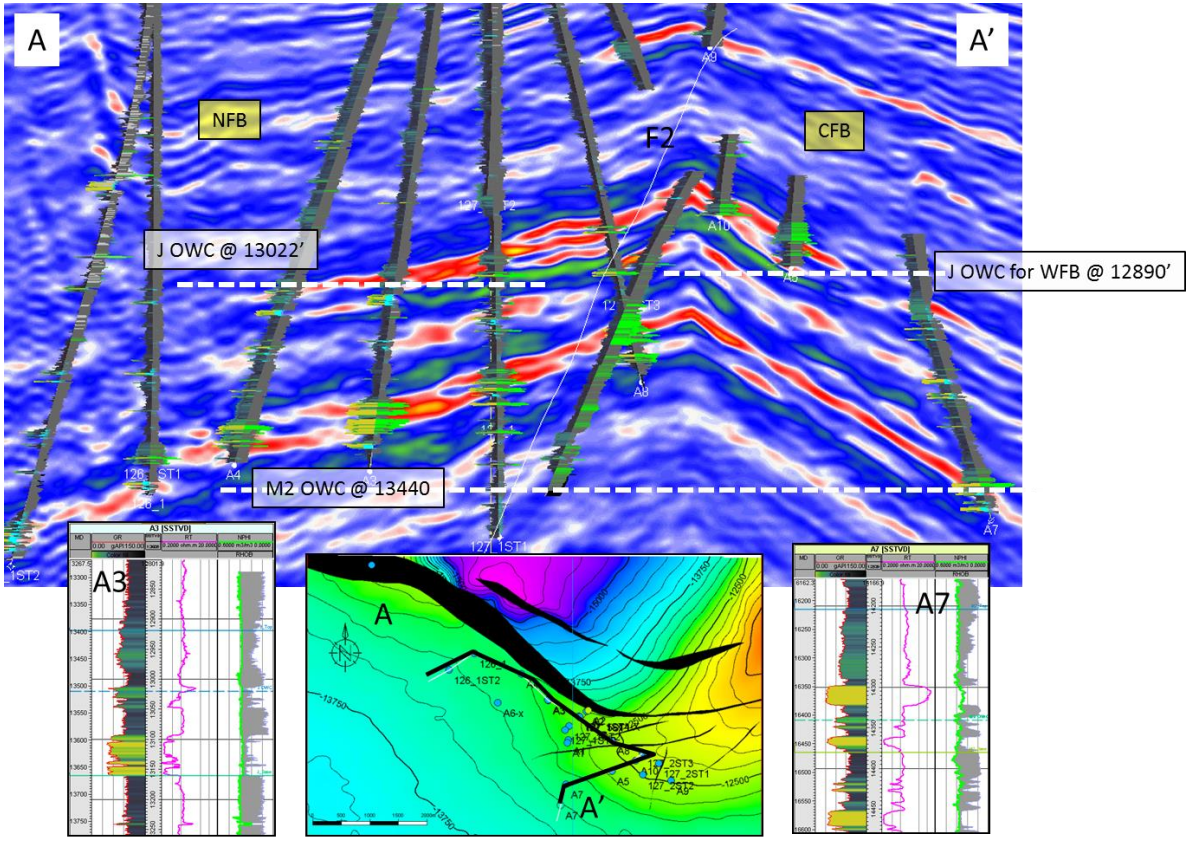

Figure 12. Seismic and well cross section showing OWC for NFB and OWC inferred for EFB; Left curve is Gamma Ray and right curve is Resistivity; dotted white line shows the inferred OWC from well log. It is also consistent with seismic amplitude distribution.

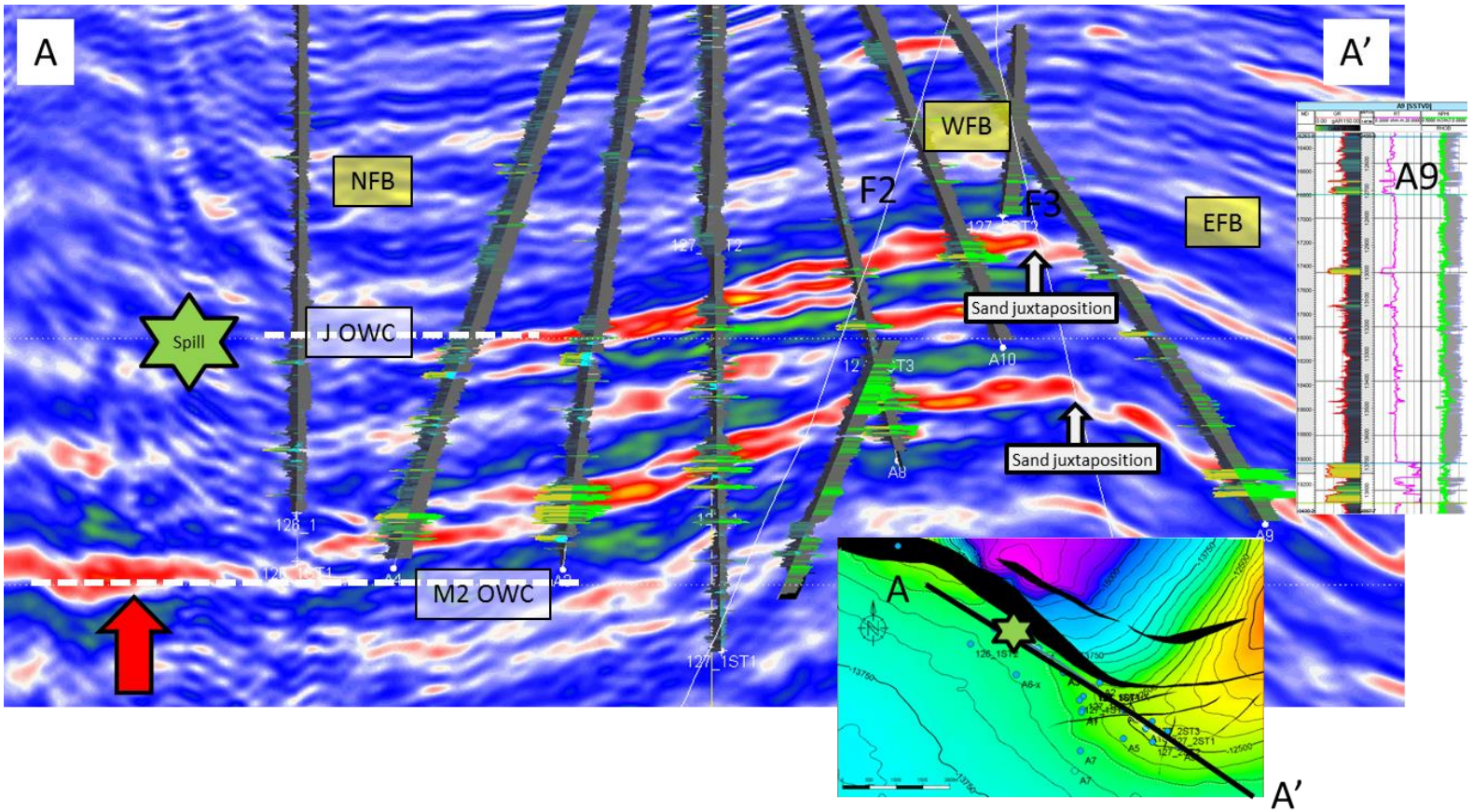

Figure 13. Seismic and well cross section (A-A') showing fluid contacts ; Left curve is Gamma Ray and right curve is Resistivity; dotted white line shows the inferred OWC from well log (Green star indicates spill point).

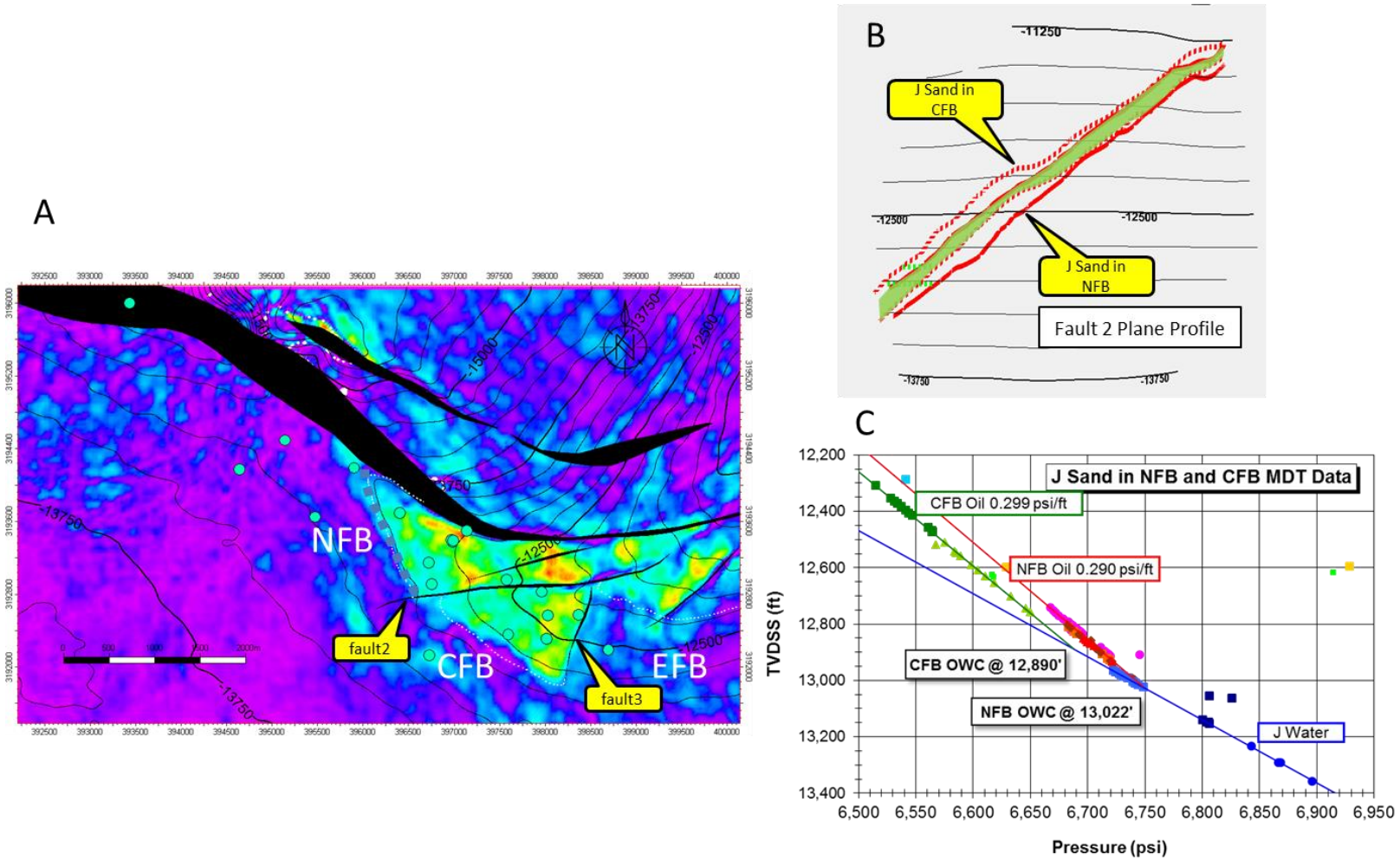

Figure 14. A) J Sand RMS Amplitude on depth structure showing faulting; B) Fault plane profile for Fault 2; Solid lines represent J sands in NFB and dashed lines are J sand top and base for CFB; Sand Juxtaposition is shaded green (top right); C) MDT pressure data showing different OWC for NFB and EFB.

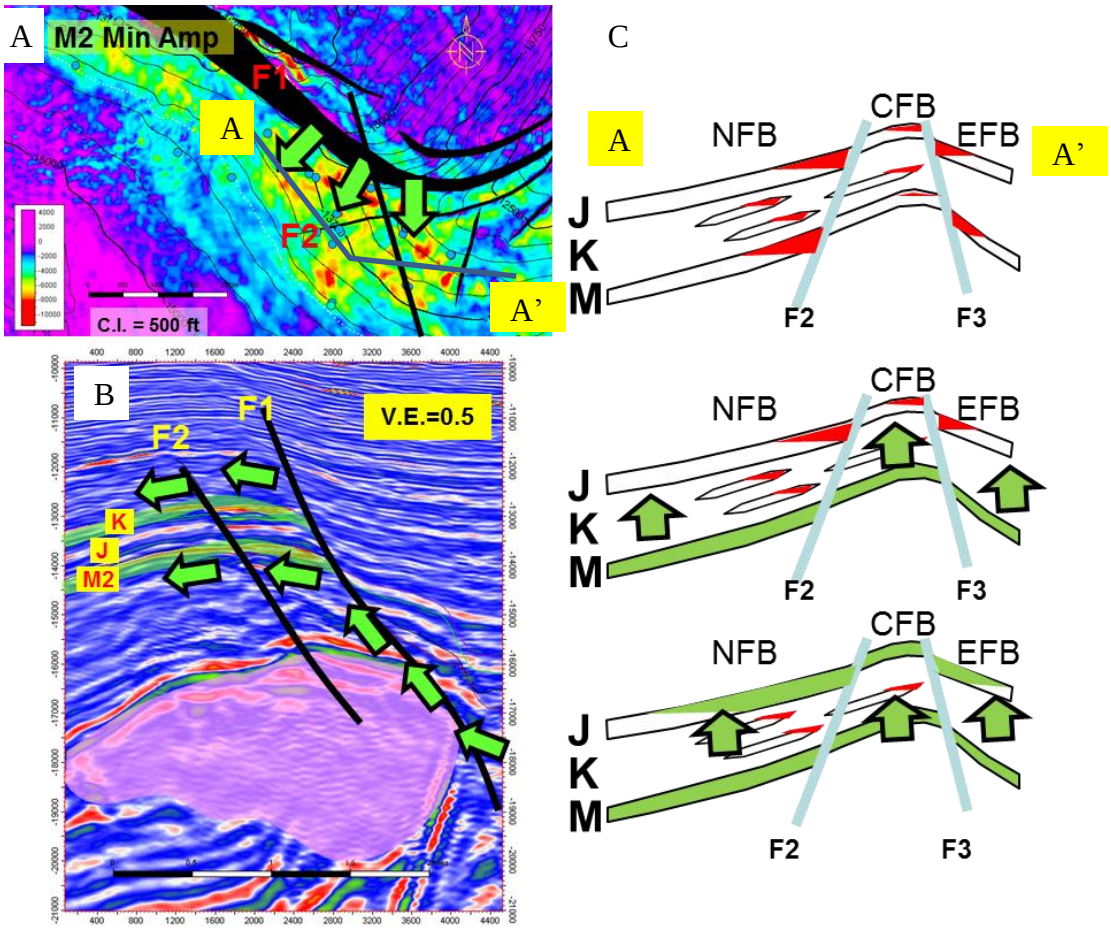

Figure 15. Charge pathway of the Horn Mountain reservoirs on A) a map view; B) cross section; C) Schematic petroleum charge history along the strike (location of the cross-section is indicated in A). C shows the presence of microbial gas prior to oil charge followed by hydrocarbon from source rock migrating up via major fault F1, charging M and J sands from north to south; K sands were bypassed due to no access to F1 conduit.

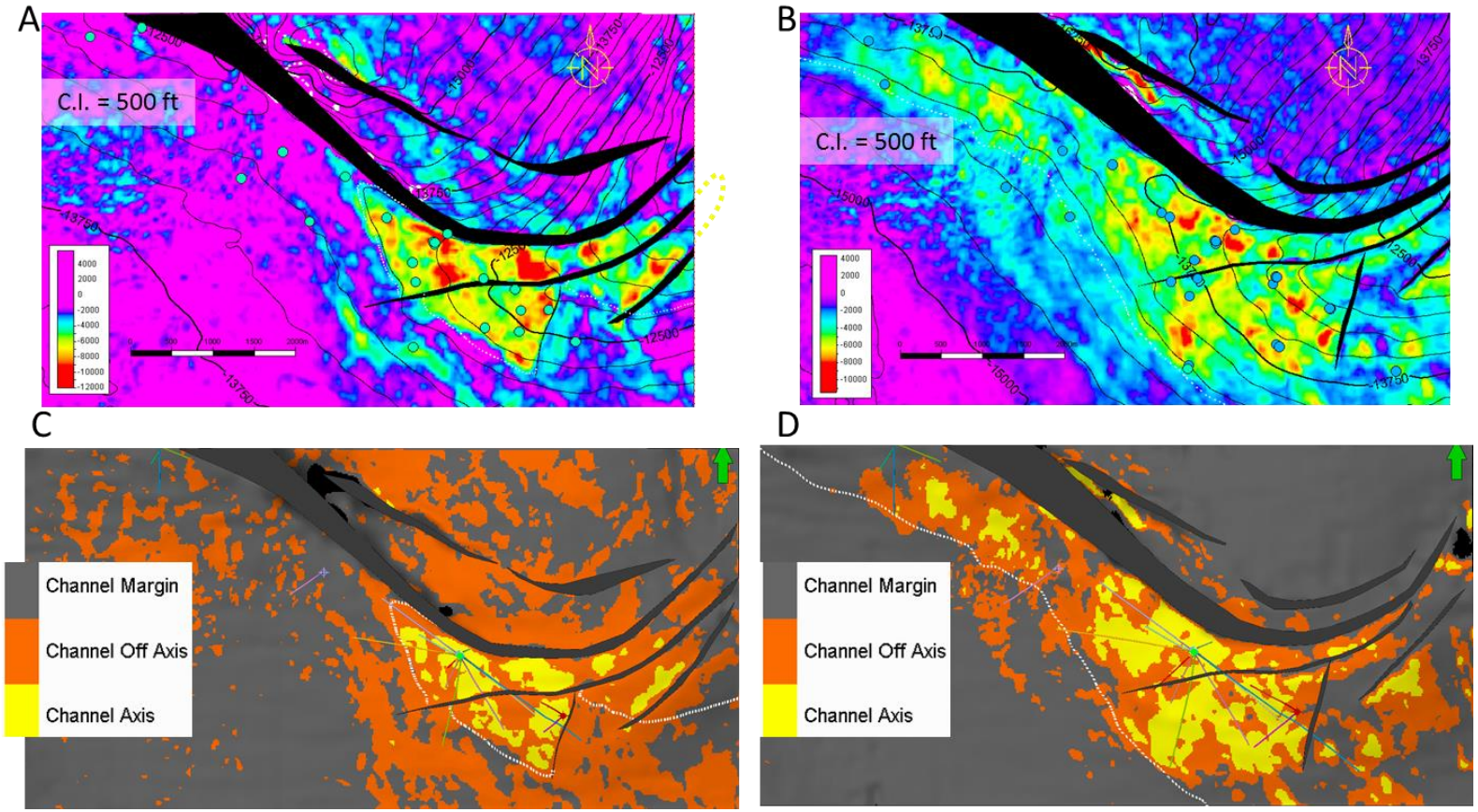

Figure 16. Correlation of N/G with Seismic Amplitude for J and M sands; A. J Sand minimum amplitude map on depth structure ; B. J sand EOD map; C. M2 sand minimum amplitude extraction map on depth structure; D. M2 sand EOD map; white dotted lines show OWC.